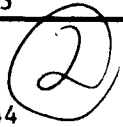
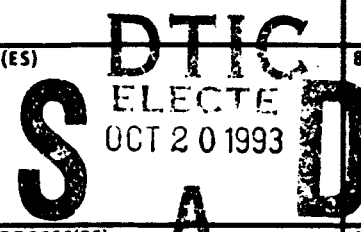


AD-A270 849

93 10 15 16 2

 Public reporting burden gathering and maintain collection of information Davis Highway, Suite 12		5E Form Approved OMB No. 0704-0188	
1. AGENCY USE ONLY (Leave blank)		2. REPORT DATE 9/9/93	
4. TITLE AND SUBTITLE First Results on InGaAsP Separate Confinement Hetero- structure Diode Lasers		3. REPORT TYPE AND DATES COVERED Interim Technical 3/15/93-9/9/93	
6. AUTHOR(S) M. Razeghi, et. al.		5. FUNDING NUMBERS DAAH04-93-G-0044 	
7. PERFORMING ORGANIZATION NAME(S) AND ADDRESS(ES) Northwestern University Center for Quantum Devices 633 Clark Street Evanston, IL 60208-1110		8. PERFORMING ORGANIZATION REPORT NUMBER  S A D	
9. SPONSORING/MONITORING AGENCY NAME(S) AND ADDRESS(ES) U.S. Army Research Office P. O. Box 12211 Research Triangle Park, NC 27709-2211		10. SPONSORING/MONITORING AGENCY REPORT NUMBER 	
11. SUPPLEMENTARY NOTES <p>The view, opinions and/or findings contained in this report are those of the author(s) and should not be construed as an official Department of the Army position, policy, or decision, unless so designated by other documentation.</p>			
12a. DISTRIBUTION/AVAILABILITY STATEMENT Approved for public release; distribution unlimited.		12b. DISTRIBUTION CODE	
13. ABSTRACT (Maximum 200 words) The first attempts of fabrication of InGaAsP/GaAs SCH-QW laser structures allowed to obtain laser diodes with threshold current densities as low as $470\text{A}/\text{cm}^2$ and differential efficiencies as high as $0.7\text{W}/\text{A}$. Long-cavity ($L \sim 1\text{mm}$) laser diodes have low series resistances of $0.1\text{-}0.4\Omega$. These diodes are suitable for testing of the properties of the Al-free material in continuous wave regime. At the same time, it is evident that further optimization of structure parameters is necessary to reach the ultimate performance expected for InGaAsP SCH QW lasers.			
14. SUBJECT TERMS GaInAsP-GaAs, High-Power Laser, Heterostructure		15. NUMBER OF PAGES 30	
		16. PRICE CODE	
17. SECURITY CLASSIFICATION OF REPORT UNCLASSIFIED	18. SECURITY CLASSIFICATION OF THIS PAGE UNCLASSIFIED	19. SECURITY CLASSIFICATION OF ABSTRACT UNCLASSIFIED	20. LIMITATION OF ABSTRACT UL

Accepted For	
NTIS	<input checked="" type="checkbox"/>
DTIC	<input type="checkbox"/>
DIA	<input type="checkbox"/>
Journal	<input type="checkbox"/>
By _____	
Distribution	
Accuracy Codes	
Dist	Avalanche Special
A-1	

DTIC QUALITY INSPECTED 2

Principal Investigator: Prof. M. Razeghi

Material growth

and characterization:	Staff	Students
	Dr. E. Kolev	X. He
	Dr. W. Carvalho	J. Hoff
	J. Gwilliam	C. Jelen
		S. Slivken

Laser processing

and measurements:	Staff	Students
	Dr. D. Garbuzov	J. Diaz
	Dr. L. Wang	I. Eliashevich
		K. Mobarhan

Theoretical calculations: X. He
H.-J. Yi

First results on InGaAsP separate confinement heterostructure diode lasers

Center for Quantum Devices, Department of Electrical Engineering and Computer Science, Northwestern University, Evanston, Illinois 60208

Abstract

The first attempts of fabrication of InGaAsP/GaAs SCH-QW laser structures allowed to obtain laser diodes with threshold current densities as low as 470A/cm^2 and differential efficiencies as high as 0.7W/A . Long-cavity ($L \sim 1\text{mm}$) laser diodes have low series resistances of $0.1 - 0.4\Omega$. These diodes are suitable for testing of the properties of the Al-free material in continuous wave regime. At the same time, it is evident, that further optimization of structure parameters is necessary to reach the ultimate performance expected for InGaAsP SCH QW lasers.

Structures and Laser Diode Fabrication

Our previous report described the fabrication and measurements of InGaAsP/GaAs Double Heterostructure (DH) laser diodes prepared by MOCVD. This report deals with the first results received with more complex Separate Confinement Heterostructure (SCH) InGaAsP/GaAs laser diodes grown by the same method as the DH diode lasers. Figure 1 shows band diagrams of a DH and a SCH structures. In the case of SCH structure there are additional waveguide layers between InGaP cladding layers, while active region thickness (L_z) is much smaller than in the case of DH diodes. The waveguide layers provide a better confinement for lasing mode, increasing its overlap with the thin active region and thus reducing the threshold current (I_{th}). Waveguide material was not doped intentionally in order to diminish internal losses and increase differential efficiency (η_d) of laser diodes. Bandgap for InGaAsP compound used as a material for waveguide layer varied from 1.6 to 1.7eV .

Table 1 shows that for wafers #66 and #76 (SCH wafers) values of L_z were approximately two times higher than for other wafers and quantum

size effect is negligible in this case. . Quantum size effects should take place in the case of SCH-SQW wafers (#71 and #79) as well as for double quantum well (SCH-DQW) wafer #77 whose active region consists of two quantum wells separated by a 100Å-thick barrier of the same composition as the waveguide layers. The waveguide layers and active region of all the structures were undoped with background impurity concentration less than 10^{17} cm^{-3} . Cladding and contact layer had the same doping levels as in the case of DH structures. A 100μm-wide stripe laser diodes for pulse testing were fabricated by the same method as in the case of DH diodes (see the previous report).

An additional solid gold metallization was deposited on a part of the wafers #66 and #71 in order to bond them p-side down on copper heatsinks and test the diodes in continuous wave (CW) operation. The diodes were indium-bonded to copper heatsinks with the In layer thickness of 3μm. In order to make this possible, a special bonding machine had been designed and manufactured, optimum temporal and thermal regimes of bonding were determined experimentally. Testing of the bonding strength confirmed its high quality: an attempt to shift a bonded diode resulted in its cracking rather than displacement.

Current-voltage characteristics

Curves 1 and 2 in Figure 2 show I-V characteristics for two diodes with L~1mm bonded n-substrate down on the heatsinks and measured under continuous current. As can be seen from the figure, series resistance for these diodes is 0.3-0.4 Ohms. The minimum resistance of 0.12 Ohms was obtained for one of long-cavity diodes of wafer #79, bonded p-side down (curve 3). A comparison of the curves 2 and 3 related to the same wafer #79 gives a possibility to suppose that in the case of n-side down bonding there is an additional component of the resistance connected with the sheet resistance of 100μm-wide stripe contact. The resistance of n-side down bonded diodes may probably be further reduced by increasing the number of contact wires (currently, two wires were used for the diodes characterized). However, the resistance obtained is already low enough to ensure continuous wave operation with high power conversion efficiency at the currents two-three times higher than threshold.

Threshold current density, differential efficiency and light-current characteristics of unbonded diodes

Table 2 summarizes parameters obtained for bonded and unbonded diodes with cavity lengths L varying from 0.3 to 1.4mm fabricated of the wafers studied. Accordingly to their cavity lengths, tested diodes were divided into three groups: first, short-cavity (SC) with $L < 0.4\text{mm}$; medium-cavity (MC) with $L = 0.5\text{-}0.7\text{mm}$; and long-cavity (LC) with $L > 1\text{mm}$. For every cavity lengths not less than three chips were measured and averaged data are presented in the Table. Three main conclusions may be derived from the data of Table 2.

- 1) The fabrication of SCH-structures has led to a considerable improvement of the laser diode parameters in comparison with DH diodes: minimum value of I_{th} decreased from 0.7kA/cm^2 for the best DH lasers to 0.47kA/cm^2 for SCH-SQW diode #79 (LC). Differential efficiency increased from 0.3W/A for DH up to $0.6\text{-}0.7\text{W/A}$ (wafers #66 and #79). Of special interest is the observation of $\eta_d=0.5\text{W/A}$ for very long cavity ($L=1.37\text{mm}$) laser diode of wafer #79. This result implies that internal losses for this wafer do not exceed $10\text{-}12\text{cm}^{-1}$.
- 2) After the bonding, parameters of LC diodes happened to be much better than for unbonded diodes of the same wavelength because of a more uniform current density distribution along the stripe for bonded diodes.
- 3) The parameters of LC diodes of wafer #66 and #79 are high enough to provide continuous wave operation of laser diodes with considerable output power.

Pulse light-current characteristics for two unbonded diodes of wafers #66 and #79 of medium cavity length are given in Figure 3. Both curves demonstrate maximum output power higher than 1.2W per facet and values of $\eta_d > 0.5\text{W/A}$ per both facets (1.3W and 0.6W/A for #79). A good reproducibility of laser diode parameters across the structure is evident from Figure 4, where a result of testing of 10 chips of wafer #66 is given.

Spectral measurements

Spectral positions of spontaneous emission bands and their half-widths as well as positions of lasing peaks for the studied laser diodes

are given in Table 3. The first two rows of Table 3 referring to the positions and half-widths of spontaneous emission bands were obtained for radiation coupled out of one of the mirrors of the diodes. The data in the next two rows are related to the radiation coupled out in the direction perpendicular to the junction plane. In case of the radiation coupled out of the mirror band maximum position is shifted to longer wavelengths and its width is reduced due to self-absorption of short-wavelength part of radiation. The value of wavelengths obtained for perpendicular registration should reflect the bandgap of active region. Figure 5 shows that in this case the electroluminescence band position and shape are very close to the photoluminescence data for the same samples. Analysing the band spectral position for diodes of different wafers we can suppose that the data for diodes of wafer #76 correspond to the 3-dimensional bandgap of active region material. Short wavelength shift of 100-150Å to the energies of 1.56-1.58eV for diodes of wafers #71 and #77 seems to be explained by the quantum-size effects in their thin active regions. A reason for long-wavelength shift for the diodes of wafers #66 and #79 is not clear now.

In order to confirm the validity of the choice of active region material composition we investigated the lasing wavelength of unbonded diodes of wafer #76 in more detail. Figures 6 and 7 show the lasing spectra of one of these diodes with cavity length 1470µm at 23°C and 31°C.

The spectra demonstrate that the wavelength which corresponds to the efficient absorption in Nd:YAG can be achieved with the chosen active region material composition. The small value of the halfwidth ($\Delta\lambda < 1$ nm) should be emphasized. This parameter is very important for design of diode-pumped Nd:YAG lasers, especially in the case of short path absorption systems

For comparison the spectrum of LPE-grown SCH-SQW InGaAsP diode #1309A-8 with approximately the same cavity length and wavelength of emission is shown in Figure 8. Notice that the broader spectra with chaotic distribution of separate lines are typical for LPE grown lasers. The half-width of total envelope for LPE grown material is not less than 2-3nm.

The exact position of the lasing wavelength is not only dependent on the material composition of the active region. It also depends on active region thickness (if active region thickness is less than 200Å), temperature, and cavity length. The dependence of lasing wavelength on cavity length for diodes of wafer #76 is plotted in Figure 9. The spectra

discussed previously correspond to one of the diodes with the longest cavity length of $1470\mu\text{m}$. The decrease of the cavity length to $340\mu\text{m}$ leads to a wavelength reduction to $0.79\mu\text{m}$. This is due to a decrease in output losses, simultaneous reduction of maximum gain, and its shift to longer wavelength.

Figure 10 shows the temperature dependence of lasing spectra maximum for a diode with the longest cavity of $1470\mu\text{m}$. The slope of linear approximation of these data is 0.2nm per degree , that is typical for AlGaAs lasers emitting at the same wavelength. Considering the results presented in these figures one can see that it is possible, through application of high reflectivity coating on one mirror facet of diodes with cavity length of about $900\mu\text{m}$, to achieve laser wavelength of 808nm at room temperature (23°C).

Continuous Wave Operation

As it is well known, in order to achieve CW operation of broad stripe contact laser diodes they are usually bonded epilayer-side down thus improving heat dissipation. Earlier in this report we mentioned that additional gold layer was deposited on the entire p-side surface of the wafers #66 and #71. Figure 11 shows schematically the metallization layers applied. According to our preliminary estimates, gold forms a Schottky barrier with moderately doped p-InGaP outside the stripe and cutoff voltage rises by 0.7V for the Schottky barrier area. Taking into account the data on series resistance of those diodes, we may suppose that a considerable current leakage through Schottky barrier could arise for LC diodes only at driving currents exceeding 5A . A comparison of threshold current for diodes of wafer #66 with and without solid gold metallization showed that there is no current leakage occurs through the Schottky barrier. Another direct confirmation of the absence of leakage is the patterns of near field of radiation for these diodes (see Figure 12). Emitting area has the same $100\mu\text{m}$ width as for the diodes without flat metallization. Photo in Figure 12 shows a laser diode bonded p-side down as described earlier in this report, with two wires connected to n-substrate.

The first results of diode testing in CW regime are shown in Figures 13 and 14a. Figure 13 shows CW lasing spectrum consisting of several well-resolved longitudinal modes, obtained for a diode of wafer #66 ($L=650\mu\text{m}$) under driving current just above the threshold. CW light-current

characteristic for this diode with the threshold current of 580mA is presented in Figure 14a. At the maximum current available from the DC current supply used (1A) CW output power was about 100mW, slope efficiency was 0.5W/A per two facets. The measurements performed in pulse regime for the same diode (Figure 14b), showed that at the driving currents exceeding 1A the slope efficiency increases approaching the value of 0.7W/A. Figure 15 shows the result of CW lifetime testing and demonstrates that no decrease in output power was observed after 20 hours of testing at 50mW output level and room temperature conditions. The aging test was terminated in order to carry out other experiments and will be continued later.

Figure 16 shows the result of testing of one of LC diodes of wafer #79 ($L=1.37\text{mm}$) in quasi-CW regime (pulse duration $8\mu\text{s}$). 200mW output power per facet was obtained at driving current 1.8A.

Conclusions

1. Threshold current density and differential efficiency.

The switching to the preparation of SCH laser diodes enabled us to decrease the threshold current density from 700 to 470A/cm^2 . The value of threshold current of about 500A/cm^2 made possible the achievement of continuous wave operation with a considerable output power , but this value of I_{th} is still detrimental to power conversion efficiency and diode lifetime. An expected value of I_{th} for SCH-SQW lasers is 3-4 times lower and additional investigation of recombination process in SCH structures is needed to discover the cause of the increased values of I_{th} for our structures.

The differential efficiency for SCH structures is twice as high as that for DH structures studied previously but still is almost 2 times lower than the upper limit expected for this type of structures. An objective of our investigation now is to find out the specific type of losses (optical or current) leading to this drawback.

2. Current-voltage characteristics.

The results presented above show that our growth and post-growth technology provide the series resistance small enough not to limit the continuous wave output power and power conversion efficiency.

3. Spectral characteristics.

The given data argue that the composition of the quaternary material of the active region is well fitted to pumping Nd:YAG lasers. The uniformity of active region material is high enough to result in the half-width of spectrum envelope as small as 0.5nm thus providing very efficient absorption of diode radiation on a short path. Further investigation of the dependence of half-width on output power will be performed for bonded diodes.

4. Continuous wave operation.

During the next phase of the project, the heatsink preparation and die mounting procedures will be the subject of special attention in order to eliminate the failures caused by these processes and ensure a possibility of accelerated testing revealing the intrinsic properties of laser structures.

FIGURE CAPTIONS

Figure 1. (a) Band diagram of a double heterostructure laser. (b) Band diagram of a separate confinement heterostructure laser.

Figure 2. CW current-voltage characteristics for two laser diodes bonded n-side down (curve 1 and 2) and for a diode bonded p-side down (curve 3).

Figure 3. Pulse light-current characteristics for diodes of wafers #66 and #79.

Figure 4. Pulse light-current characteristics of 10 diodes of wafer #66 ($L=710\mu m$).

Figure 5. A comparison of photoluminescence spectrum of wafer #71 (solid line) and electroluminescence spectra of a diode of the same wafer. Dashed and broken curves refer to the radiation coupled out in the direction parallel and perpendicular to the junction plane, respectively.

Figure 6. The lasing spectrum for a diode of wafer #79 with cavity length 1.47mm at 23°C.

Figure 7. The lasing spectrum for a diode of wafer #79 with cavity length 1.47mm at 31°C.

Figure 8. The lasing spectrum of LPE-grown diode #1309A-8 with cavity length 0.9mm at 16°C.

Figure 9. Lasing wavelength dependence on cavity length for diodes of wafer #76 at 23°C.

Figure 10. Temperature dependence of the lasing wavelength for a diode of wafer #76 with cavity length 1.47mm.

Figure 11. Scheme of metallization for the diodes with solid gold deposited on p-side.

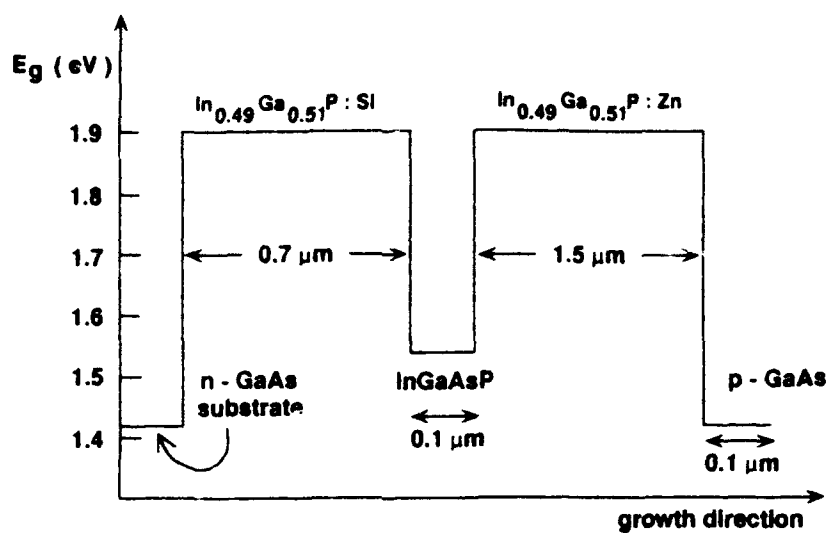
Figure 12. Diode bonded p-side down and the distribution of spontaneous emission intensity along the mirror facet. An unbonded diode is also shown p-side up to demonstrate the stripe width in this scale.

Figure 13. CW lasing spectrum for a diode of wafer #66 just above the threshold.

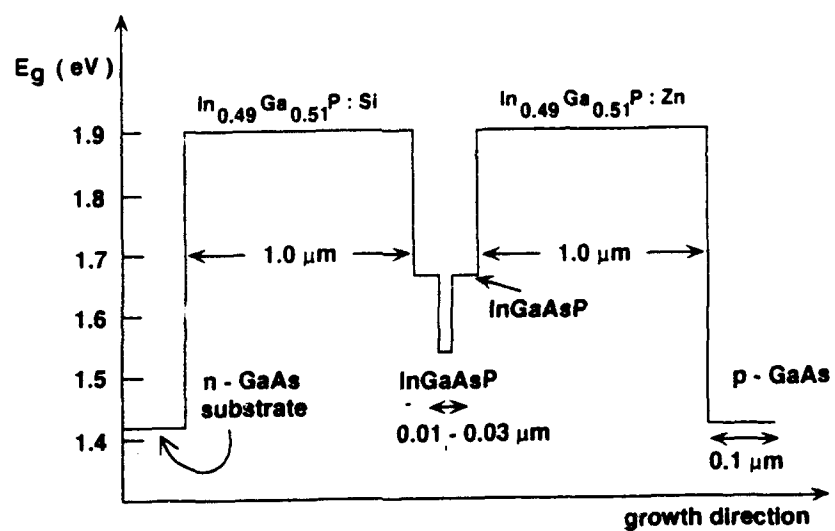
Figure 14. (a) CW light-current characteristic for a diode of wafer #66 with $L=650\mu m$. (b) Pulse light-current characteristic for the same diode.

Figure 15. Preliminary results of lifetime testing for a diode of wafer #66 under driving current 810mA at room temperature (output power 50mW).

Figure 16. Quasi-CW light-current characteristic for a diode of wafer #79 with $L=1.37mm$ (pulse duration 8 μs , frequency 400Hz).



(a)



(b)

Figure 1. (a) Band diagram of a double heterostructure laser.
 (b) Band diagram of a separate confinement heterostructure laser.

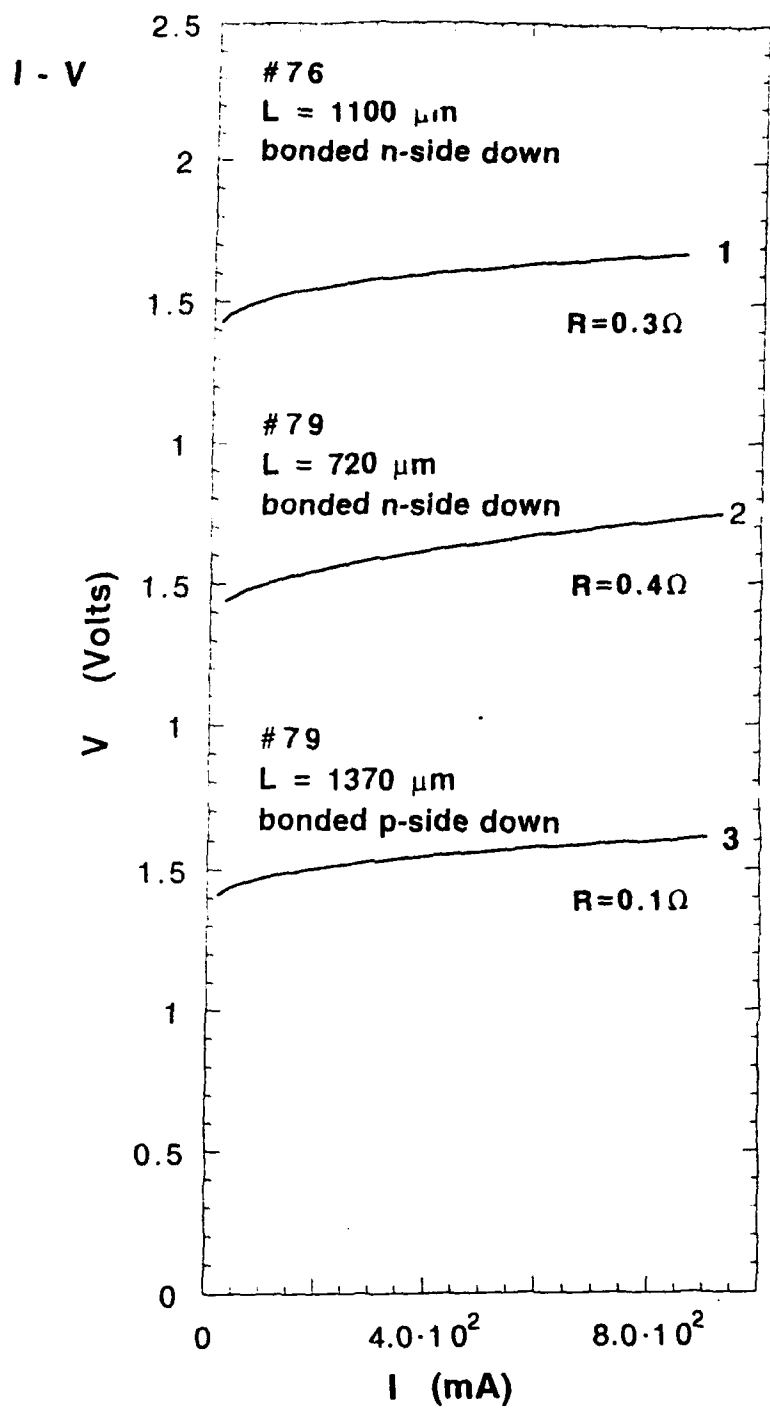


Figure 2. CW current-voltage characteristics for two laser diodes bonded n-side down (curve 1 and 2) and for a diode bonded p-side down (curve 3).

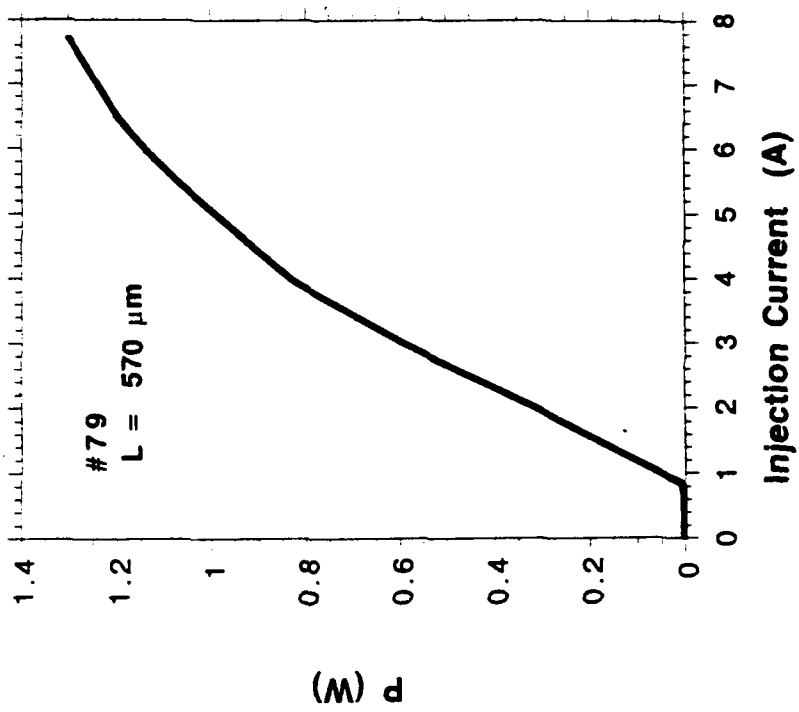
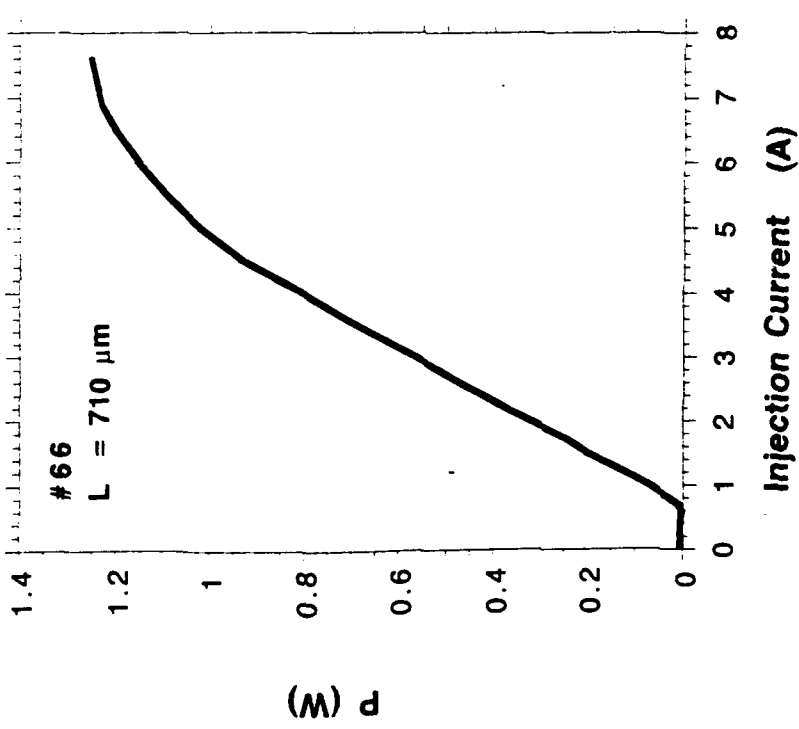


Figure 3. Pulse light-current characteristics for diodes of wafers #66 and #79.

(a) (b)

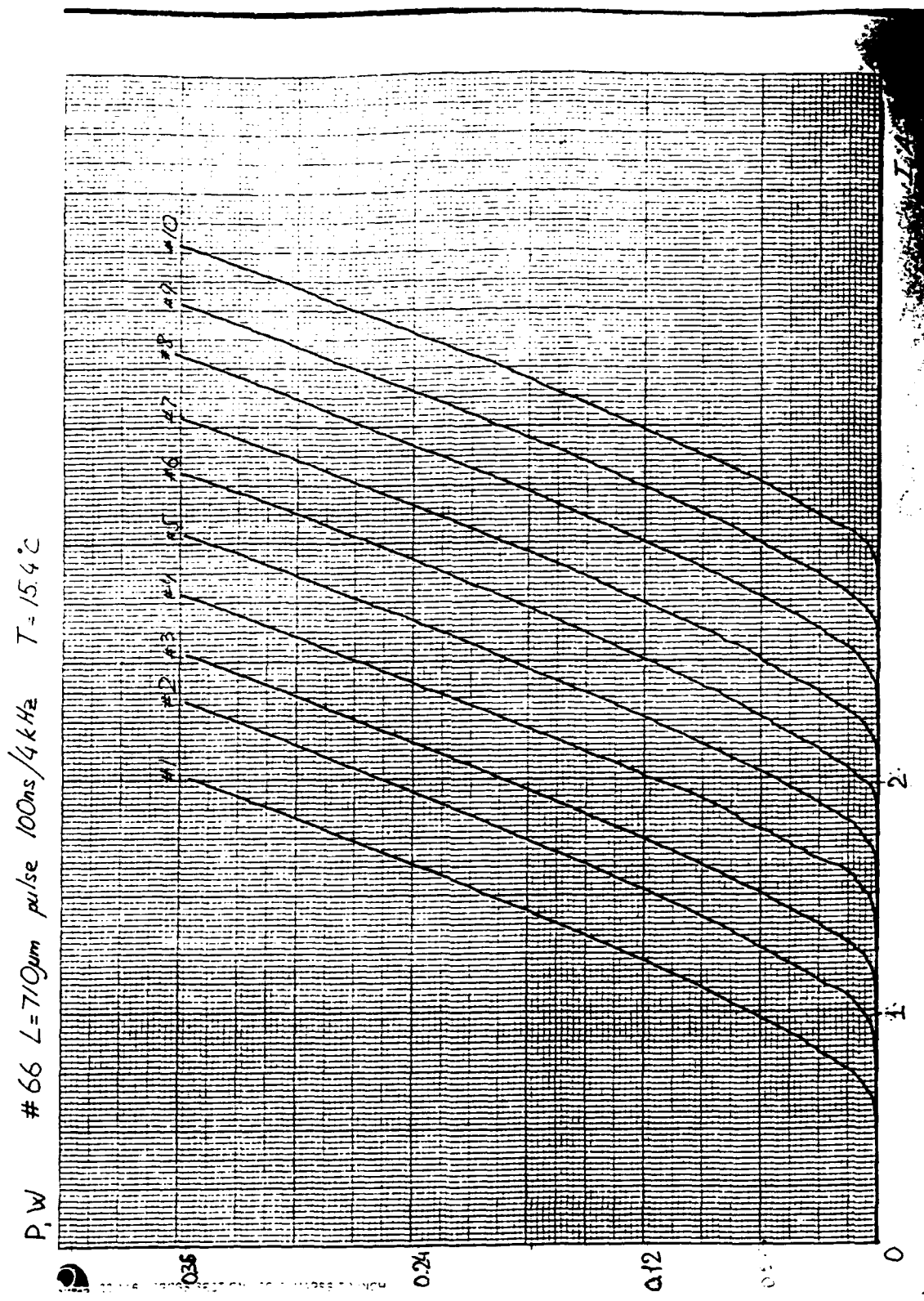


Figure 4. Pulse light-current characteristics of 10 diodes of wafer #66 (L=710μm).

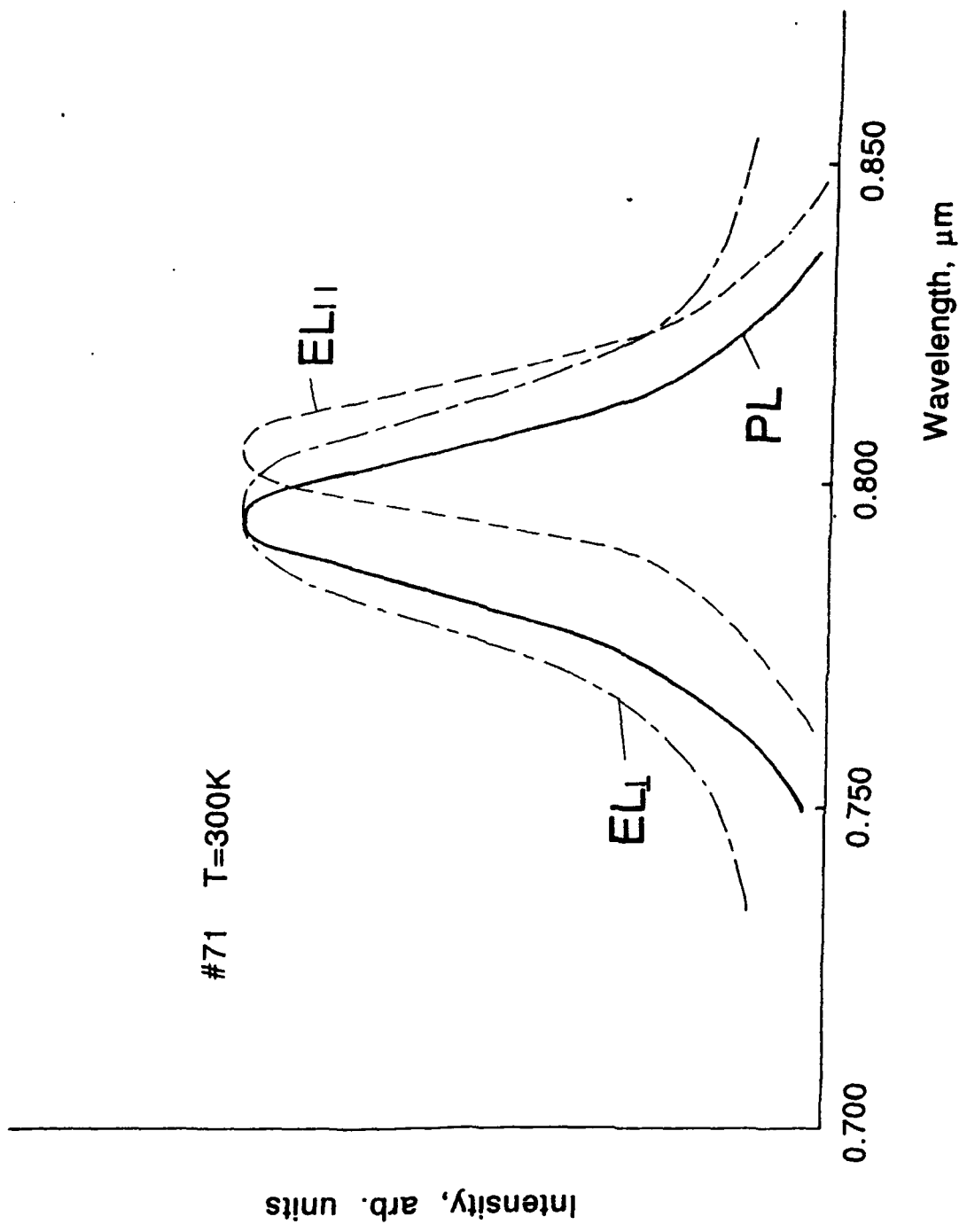


Figure 5. A comparison of photoluminescence spectrum of wafer #71 (solid line) and electroluminescence spectra of a diode of the same wafer. Dashed and broken curves refer to the radiation coupled out in the direction parallel and perpendicular to the junction plane, respectively.

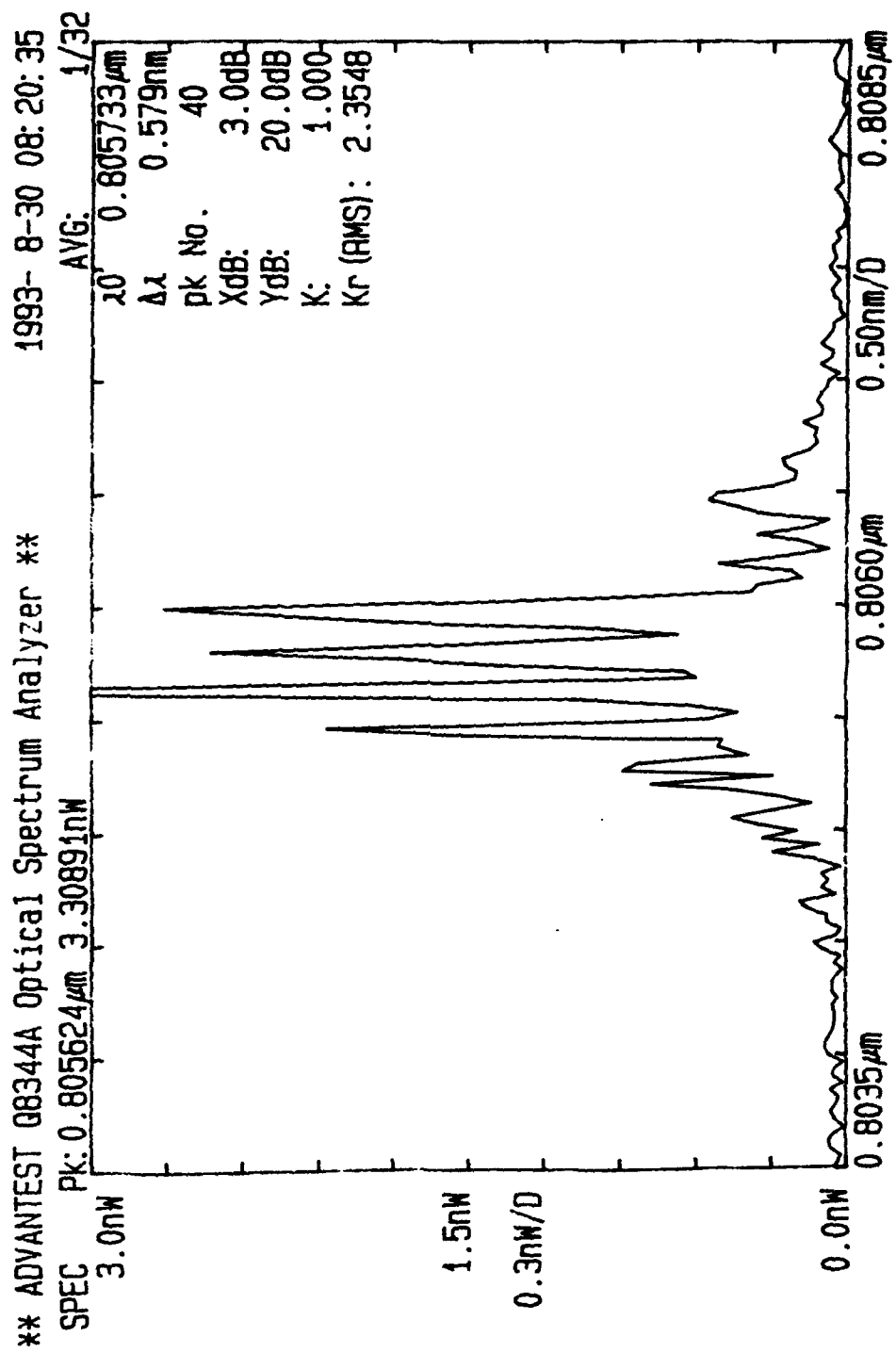


Figure 6. The lasing spectrum for a diode of wafer #79 with cavity length 1.47mm at 23°C.

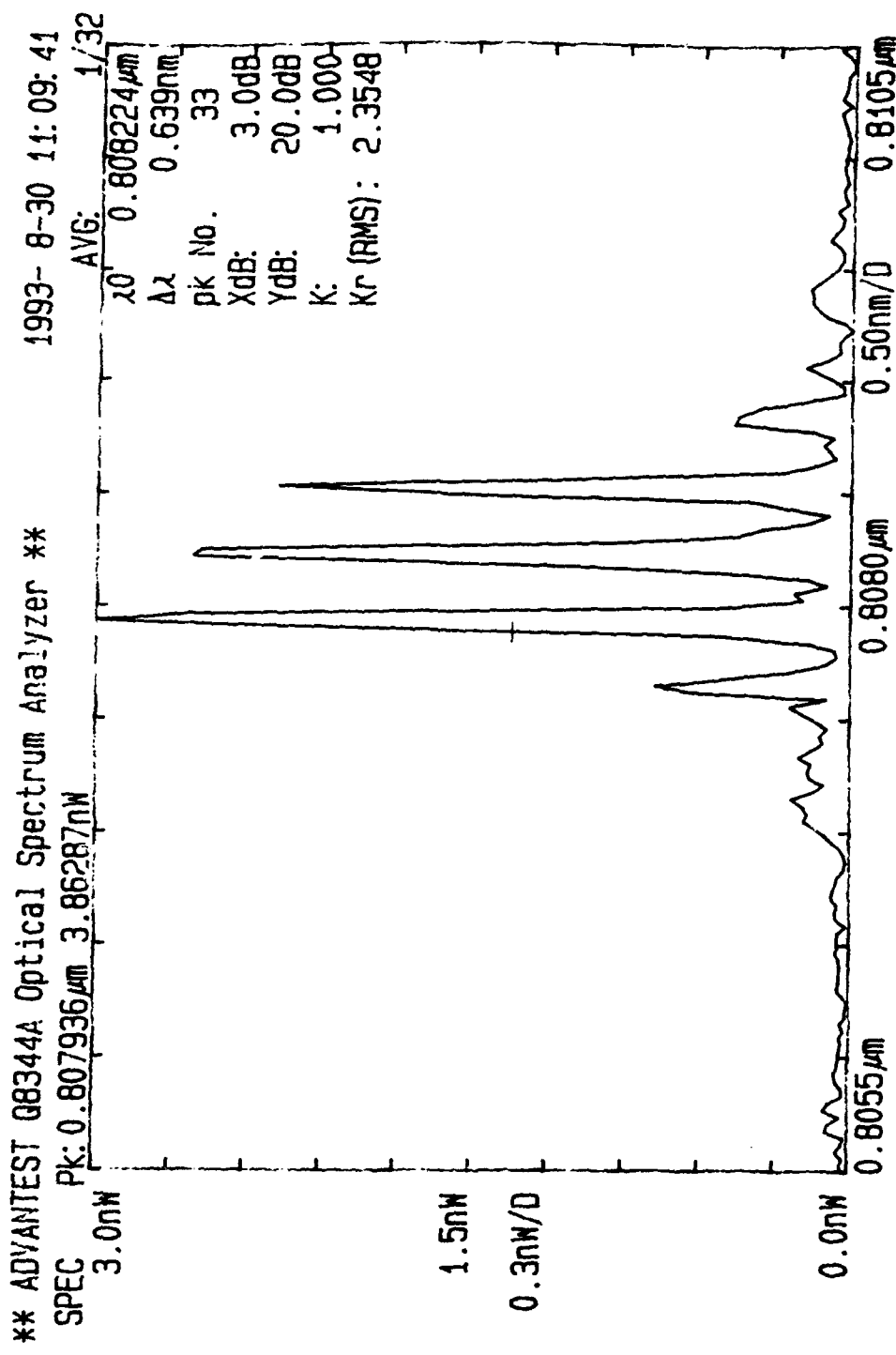


Figure 7. The lasing spectrum for a diode of wafer #79 with cavity length 1.47mm at 31°C.

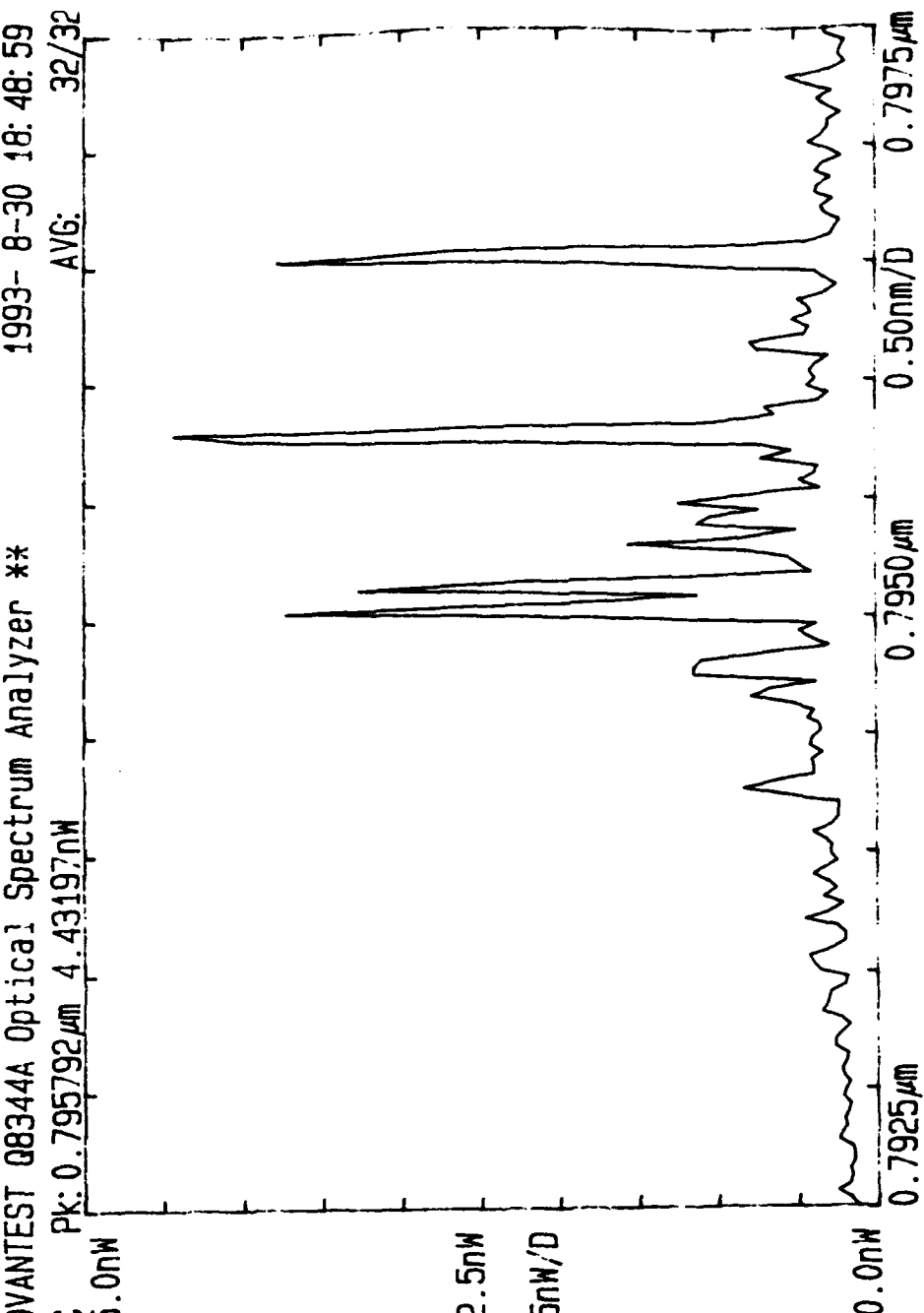


Figure 8. The lasing spectrum of LPE-grown diode #1309A-8 with cavity length 0.9mm at 16°C.

Wavelength vs. Cavity Length

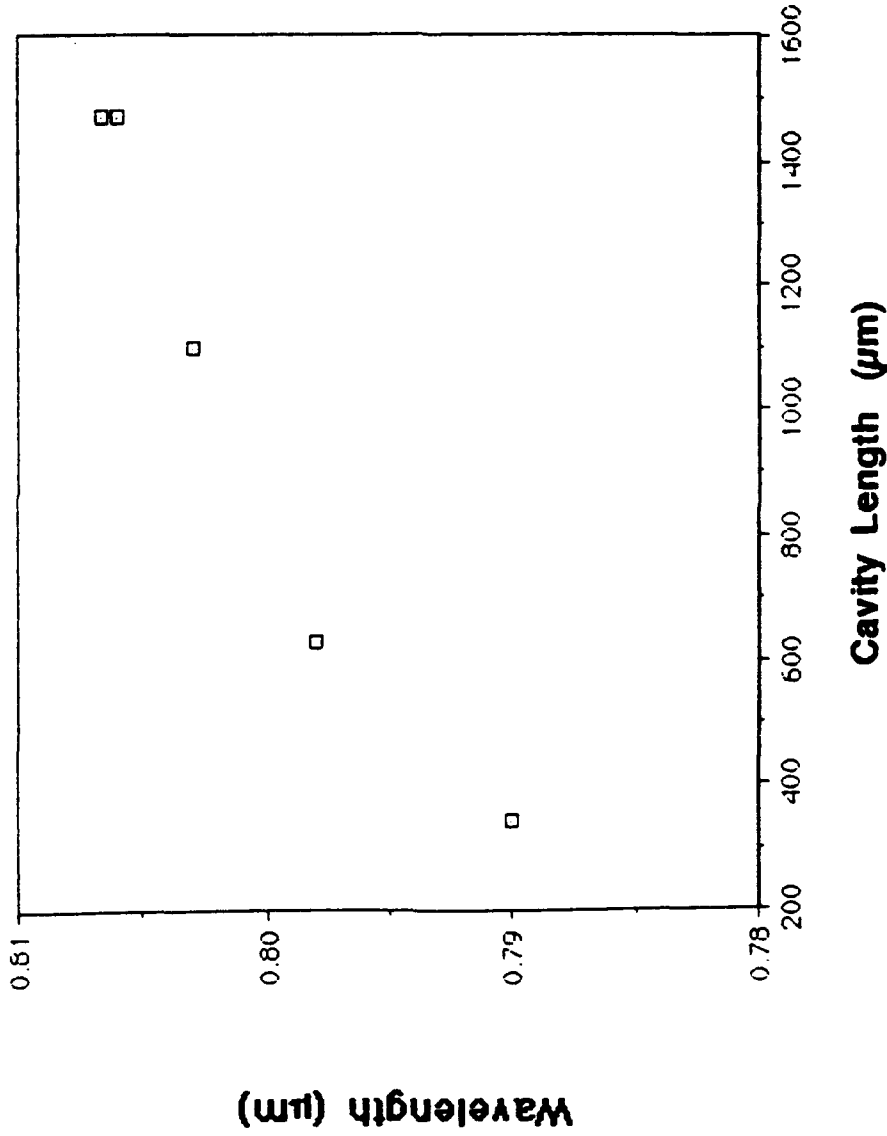


Figure 9. Lasing wavelength dependence on cavity length for diodes of wafer #76 at 23°C.

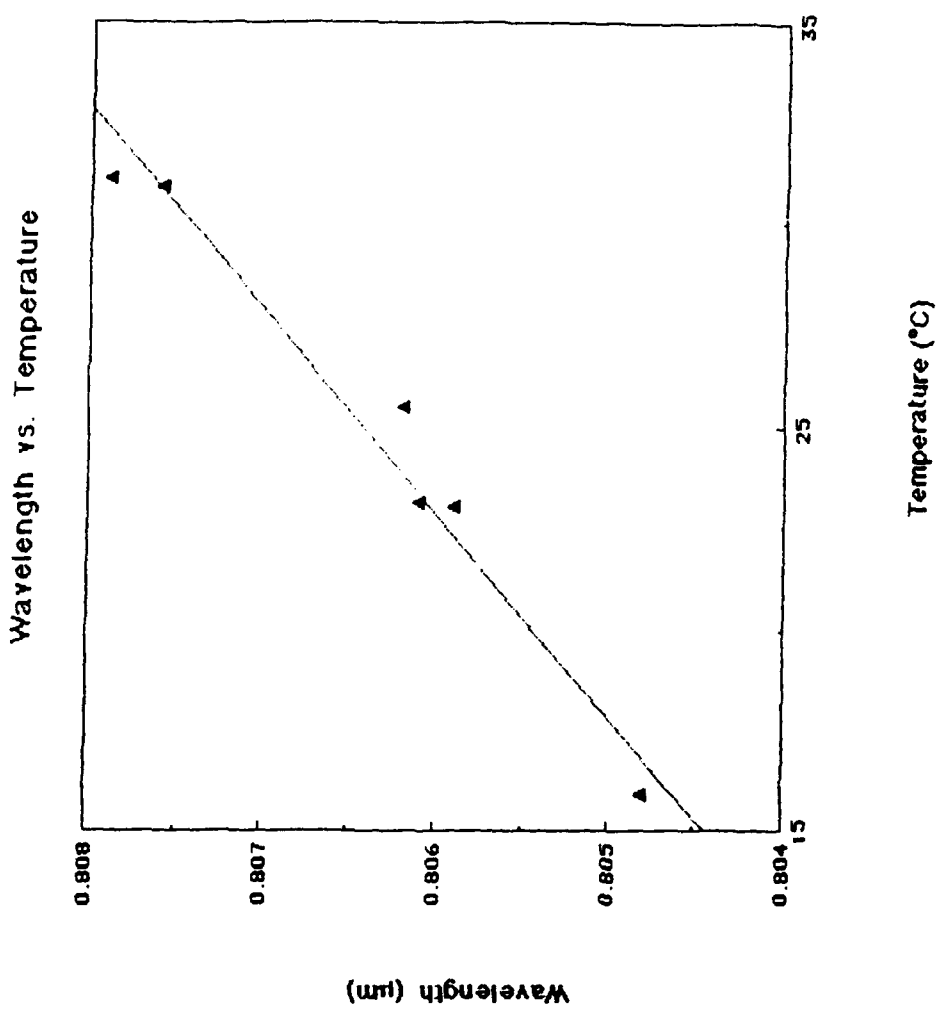


Figure 10. Temperature dependence of the lasing wavelength for a diode of wafer #76 with cavity length 1.47mm.

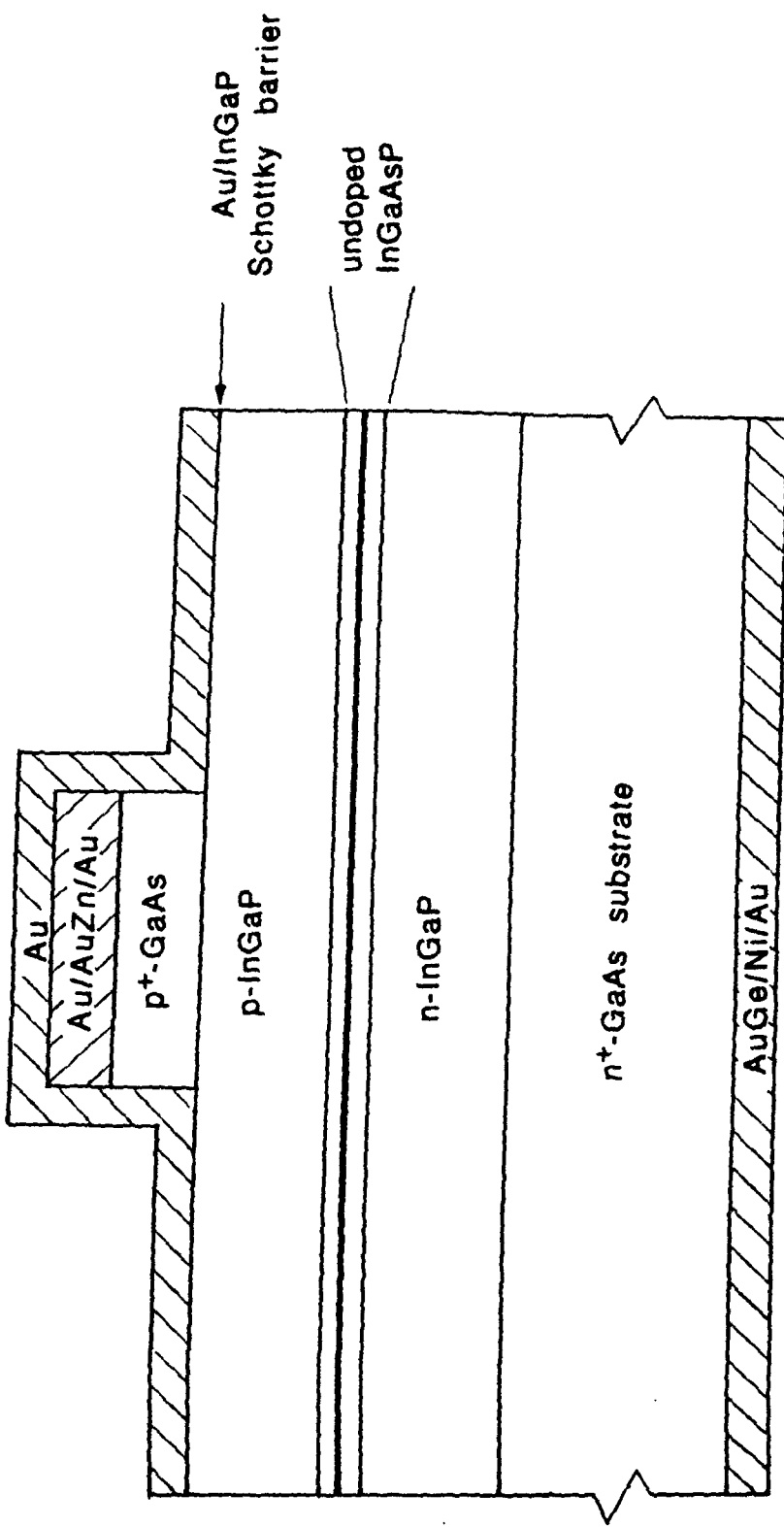


Figure 11. Scheme of metallization for the diodes with solid gold deposited on p-side.

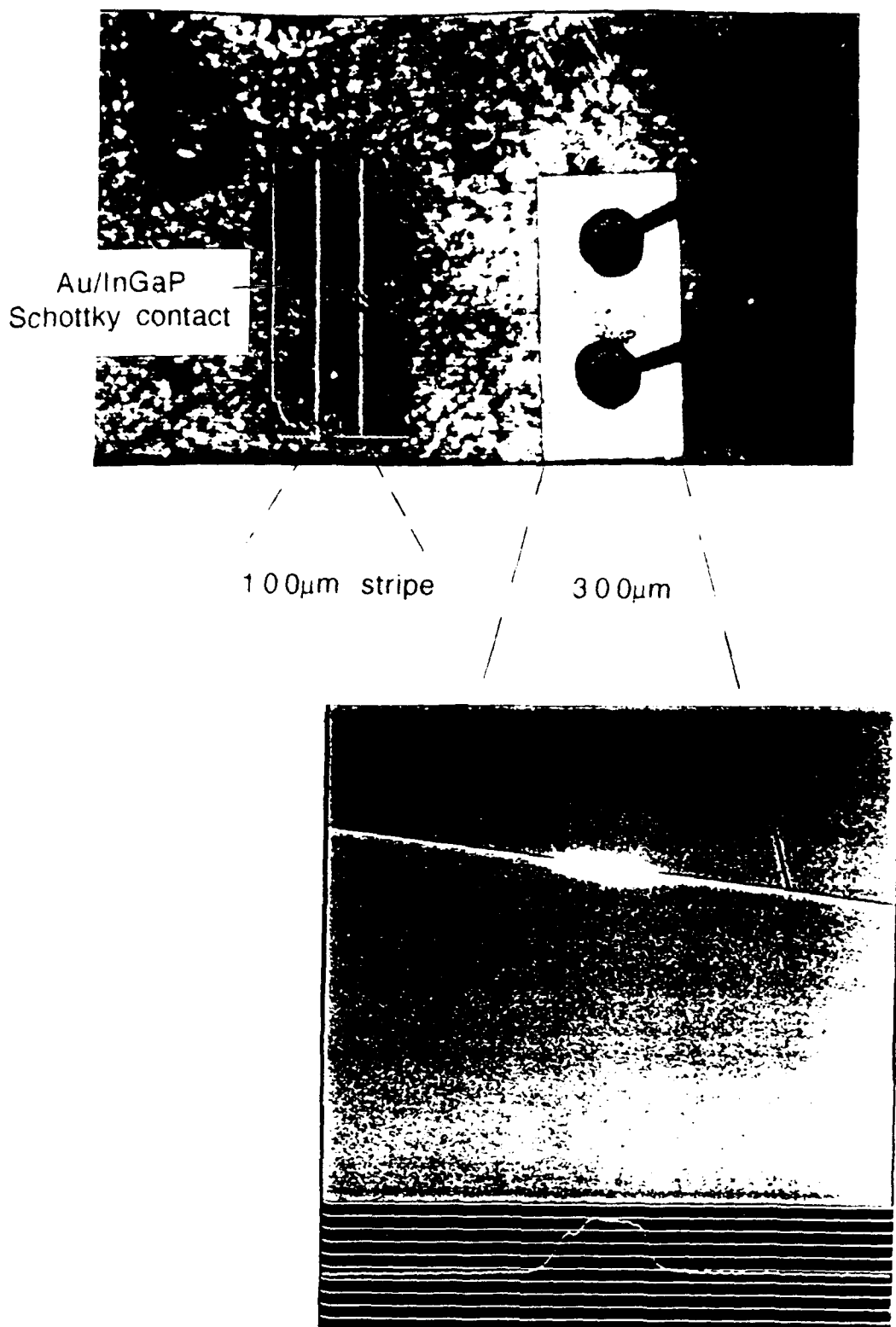


Figure 12. Diode bonded p-side down and the distribution of spontaneous emission intensity along the mirror facet. An unbonded diode is also shown p-side up to demonstrate the stripe width in this scale.

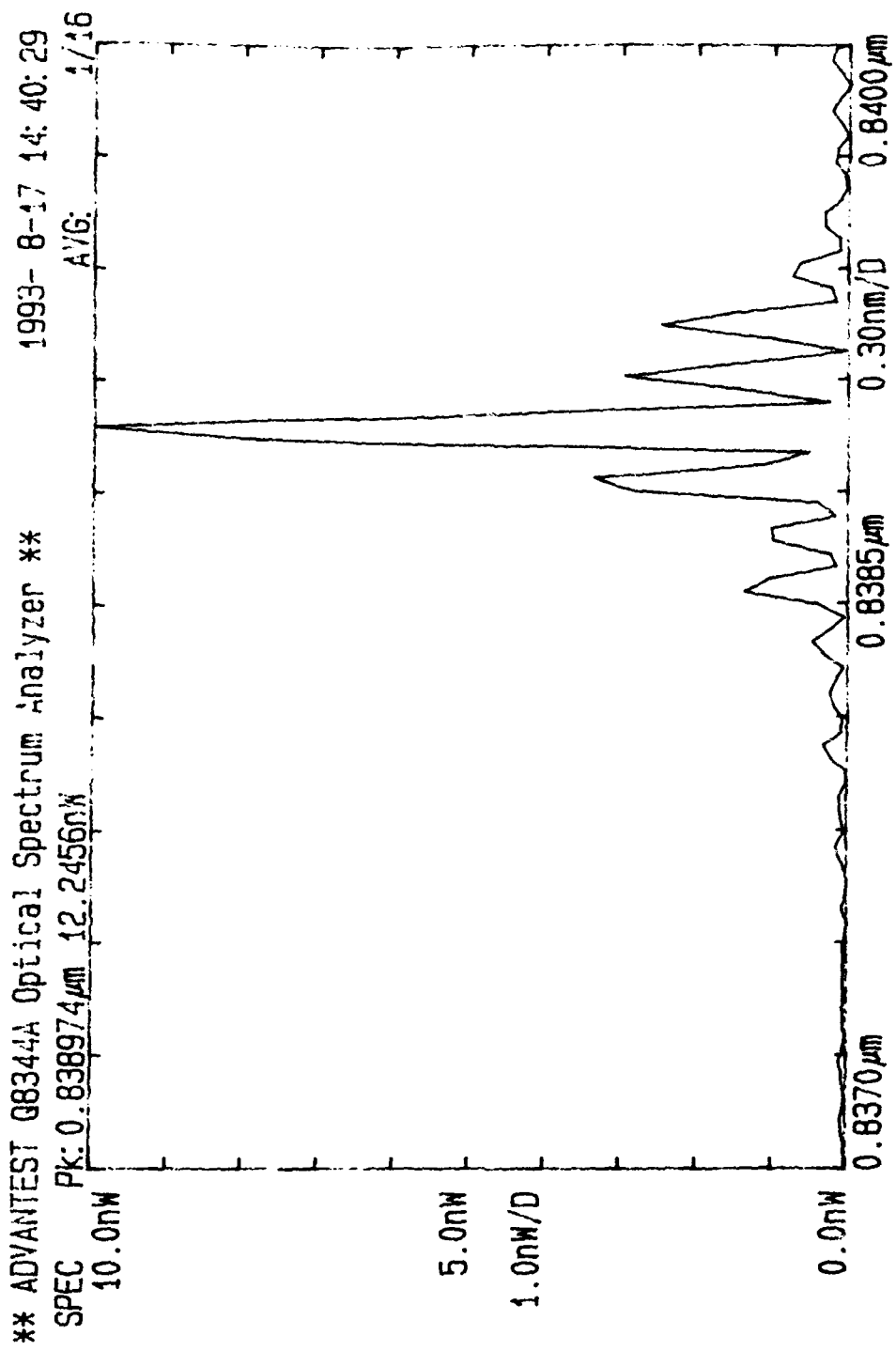


Figure 13. CW lasing spectrum for a diode of water #66 just above the threshold.

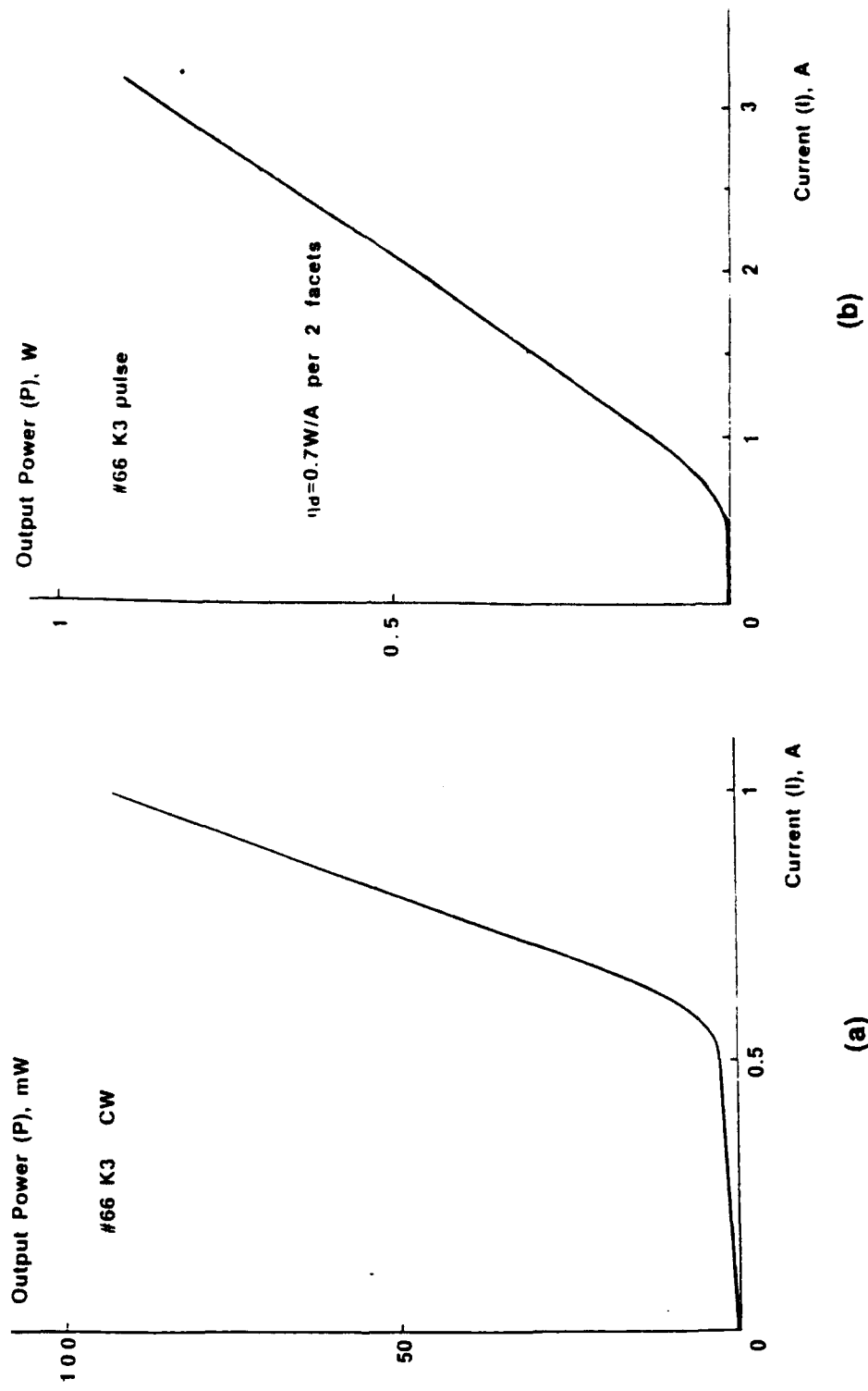


Figure 14. (a) CW light-current characteristic for a diode of wafer #66 with $L=650\mu\text{m}$. (b) Pulse light-current characteristic for the same diode.

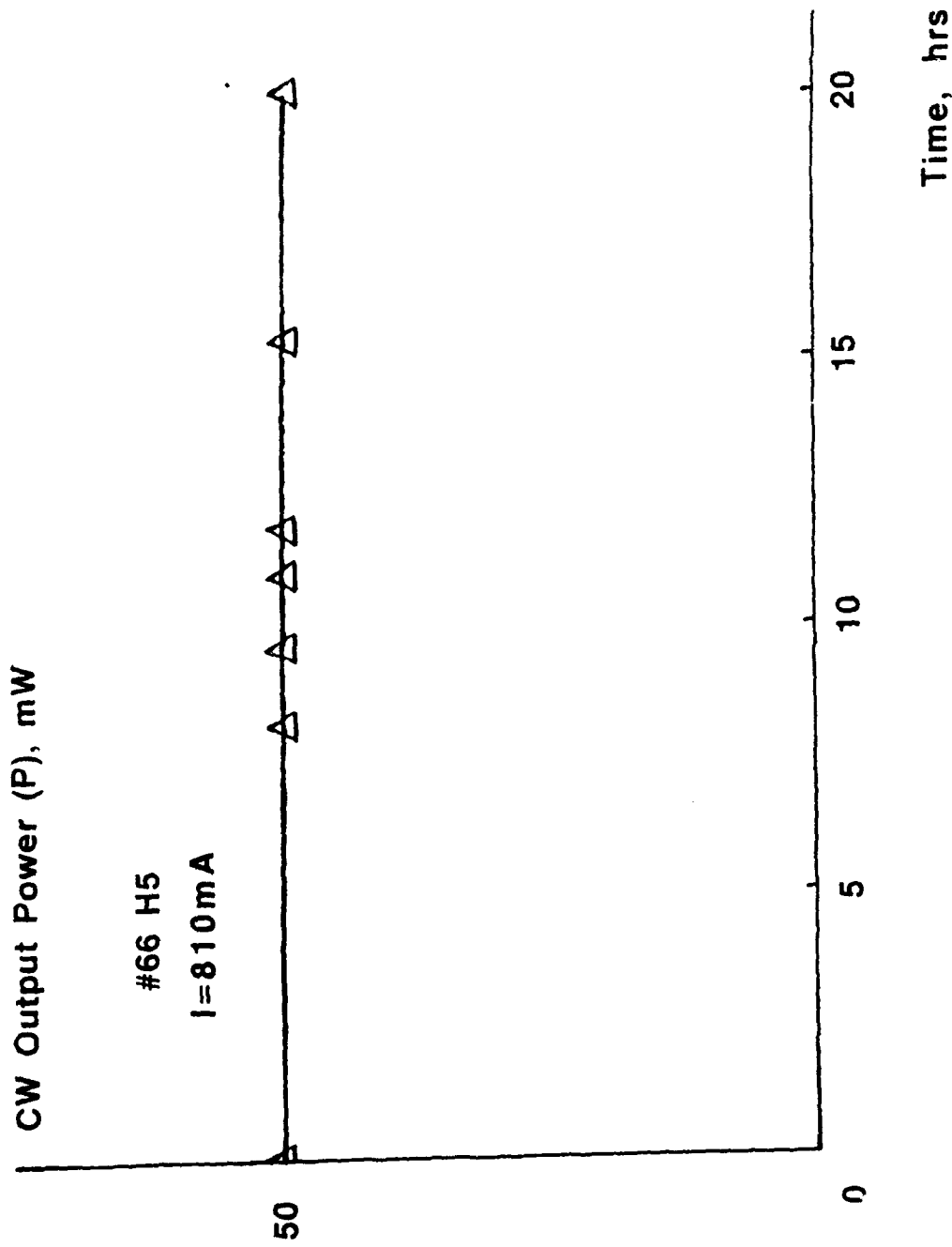


Figure 15. Preliminary results of lifetime testing for a diode of wafer #66 under driving current 810mA at room temperature (output power 50mW).

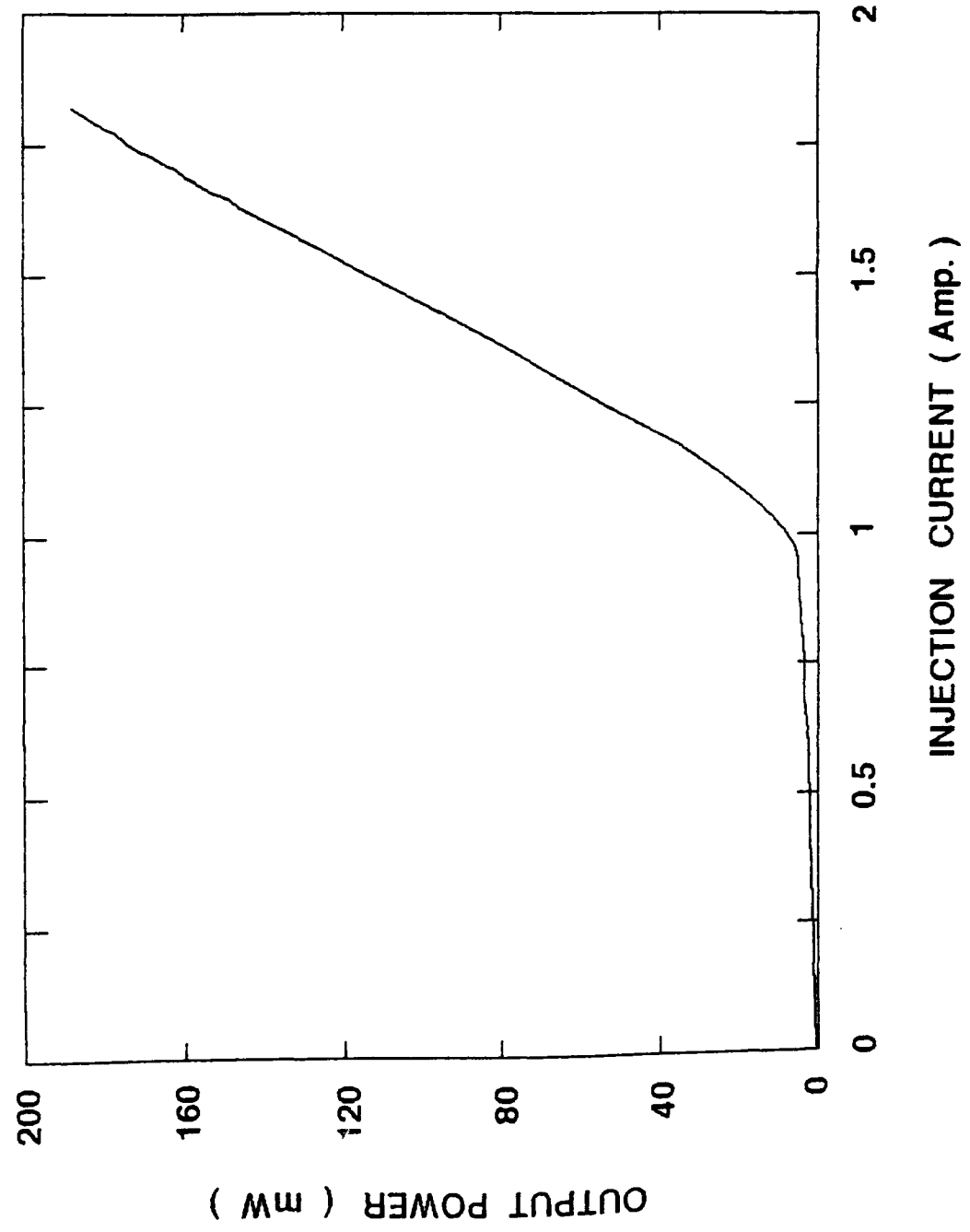


Figure 16. Quasi-CW light-current characteristic for a diode of wafer #79 with L=1.37mm (pulse duration 8 μ s, frequency 400Hz).

Table 1. List of wafers used for laser diode fabrication.

	SCH		SCH-SQW		SCH-DQW
	#66	#76	#71	#79	#77
active layer thickness, Å	300	300	150	150	2x150

Table 2.

Parameters	#66		#71		#76		#77		#79
Cavity length	SC	MC	LC	SC	MC	LC	SC	MC	LC
I _{th} , kA/cm ²	1.30	0.75		1.30	0.75	0.50	1.50	0.80	1.60
I _{th(b)} , kA/cm ²	0.80	0.50							
η _d , W/A	0.55	0.55		0.20	0.30	0.20	0.12	0.35	
η _{d(b)} , W/A		0.70	0.40						

Abbreviations:

SC - Short Cavity L = 300 - 400 μm
 MC - Medium Cavity L = 500 - 700 μm
 LC - Long Cavity L = 1000 - 1500 μm

I_{th(b)}, η_{d(b)} - data for bonded diodes.

Table 3. Spectral measurements data.

	SCH		SCH-SQW		SCH-DQW
	#66	#76	#71	#79	#77
$\lambda_{\text{spont. II}}, \text{\AA}$	8660	8180	8080	8300	8020
FWHM, nm	40	20	20	29	43
$\lambda_{\text{spont.}}, \text{\AA}$	8400	8100	7930	8220	
FWHM, nm	55	40	38	65	
$\lambda_{\text{gen. (LC)}}, \text{\AA}$	8380	7987	7900	8240	7850
$\lambda_{\text{gen. (SC)}}, \text{\AA}$	8310			8115	

$\lambda_{\text{spont. II}}$: Position of spontaneous emission band maximum for radiation coupled out through one of the mirrors

$\lambda_{\text{spont.}}$: Position of spontaneous emission band maximum for radiation coupled out in the direction perpendicular to the junction plane.

$\lambda_{\text{gen. (LC)}}$ Position of lasing peak for long-cavity laser diodes.

$\lambda_{\text{gen. (SC)}}$ Position of lasing peak for short-cavity laser diodes.

InGaAsP Diode Laser for Nd:YAG Pumping

ARPA/US Army project # DAAH 04-93-G-0044

Principal Investigator: Prof. M. Razeghi

	Yesterday	Today	Tomorrow
Laser structure	DH	SCH	SCH-QW
I _{threshold} , A/cm ²	700	470	<200
η _d , W/A (per 2 facets)	0.4	0.7	>1.0
P _{output} (per facet)	150mW pulse	1.3 W pulse, 100mW CW	>1W CW
Lifetime	Not tested	Tested up to 20 hrs	>1000 hrs